Two-layer Q_S structure of the slab near the southern Kurile trench

Takahiro Maeda[1] and Tsutomu Sasatani[2]

[1]*Institute of Seismology and Volcanology, Graduate School of Science, Hokkaido University, N10W8 Kita-ku, Sapporo 060-0810, Japan*
[2]*Division of Earth and Planetary Sciences, Graduate School of Science, Hokkaido University, N10W8 Kita-ku, Sapporo 060-0810, Japan*

We estimate Q_s values (quality factor for S-wave) of the slab near the southern Kurile trench by using seismic data observed at ocean bottom seismometer (OBS) stations from selected local earthquakes. The seismic rays pass mainly through the slab and this enable us to directly estimate the slab Q_s values. The spectral inversion and coda normalization method are applied to these data. The estimated Q_s values from the two methods are nearly the same and increase with frequencies. However, these Q_s values are not high enough to explain the abnormal distribution of ground motion that has been recognized as abnormal distribution of seismic intensities at the Japanese arc. Thus we propose a two-layer Q_s structure of the slab to explain the both facts, our slab Q_s values and the abnormal distribution of ground motion. The two-layer Q_s structure consists of the upper layer with not so high Q_s values ($39f^{1.0}$) and lower layer with very high Q_s values ($500f^{1.0}$); the upper layer has a thickness of about 50 km. Seismic activity is restricted only within the upper layer of the two-layer Q_s structure. This may mean that the two-layer Q_s structure reflects the different material property between the upper and lower layer of the slab.
Key words: Two-layer Q_s structure of the slab, Spectral inversion method, Coda normalization method, Abnormal distribution of seismic intensities.

1. Introduction

It is well known that there exists the anomalous upper mantle structure beneath island-arc regions; the high Q and high velocity zone, that is, the descending plate or slab sinks into the low Q and low velocity upper mantle (e.g., Utsu, 1967). This anomalous structure has been originally deduced from abnormal seismic intensity distribution and travel time studies of P- and S-wave from nearby deep earthquakes at the Japanese island-arc. Subsequently the three-dimensional (3-D) attenuation structure beneath the Japanese island-arc has been estimated by using seismic records (e.g., Umino and Hasegawa, 1984; Nakamura and Uetake, 2000; Tsumura *et al.*, 2000). These studies, however, used seismic data recorded at land stations. In this case, the seismic rays pass through not only the slab but also a zone outside the slab. This means that the resolving power for estimating the slab Q values using these data is not so high though above studies have concluded that the high Q regions generally correspond to the slab.

In this study, we estimate the slab Q_s values (Q values for S-wave) near the southern Kurile trench by using the seismic data recorded at ocean bottom stations. For these data, the seismic rays pass mainly through the slab and this enable us to directly estimate the slab Q_s values with the high resolving power. The estimated Q_s values, however, are not so high and these values cannot explain the abnormal distribution of seismic intensities observed around the southern Kurile arc. This means that the slab has a complex Q_s structure. Consequently we propose a two-layer Q_s structure of the slab to explain the both facts, our slab Q_s values and the observed abnormal distribution of seismic intensities. The two-layer Q_s structure consists of the upper layer with not so high Q_s values and the lower layer with very high Q_s values; the upper layer has a thickness of about 50 km. Finally we briefly discuss the tectonic implications of the two-layer Q_s structure of the slab.

2. Estimation of the Slab Q_S Values

A real time seafloor cabled observation system has been installed in July, 1999 by the Japan Agency for Marine-Earth Science and Technology (JAMSTEC) at the continental slope in the southern Kurile subduction zone approximately 100 to 150 km off the southern Hokkaido coast (Hirata *et al.*, 2002) (Fig. 1). This system has three ocean bottom seismometer (OBS) stations and each station has a three-component acceleration detector. The waveform data are recorded at 100 samples/sec and the effective resolution is about 22 bits. These data provide a good opportunity to directly estimate the slab Q_s values near the southern Kurile trench.

2.1 Method

The amplitude spectrum of direct S-wave ($O_{ij}(f)$) can be expressed as

$$O_{ij}(f) = S_i(f)P_{ij}(f)G_j(f) \qquad (1)$$

where $S_i(f)$, $G_j(f)$ and $P_{ij}(f)$ represent the source spectrum of the i-th event, the site amplification factor at the j-th station and the path effect between the i-th event and
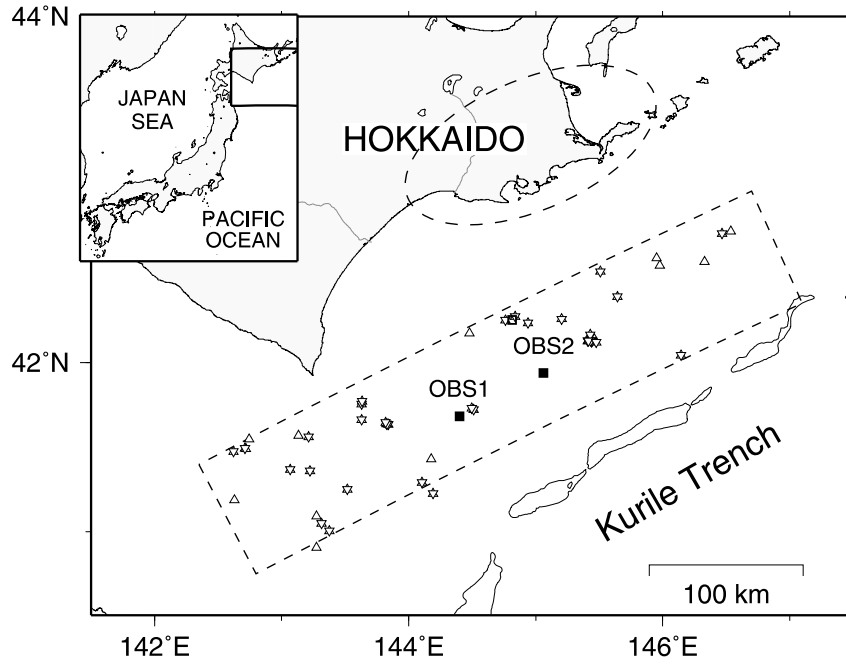
Fig. 1. Location map showing epicenters and ocean bottom seismometer (OBS) stations (solid squares) used in this study. Open triangles and inverted triangles are earthquakes used in the SI method and CN method, respectively. We select the earthquakes occurring in a narrow belt enclosed by broken lines for estimation of the slab Q_s values. A broken ellipsoid shows the study area for the fore-arc side mantle wedge (Maeda, 2003). Map inset shows the study area (the southern Kurile arc).

the j-th station, respectively. Although these factors may be dependent on a source-receiver direction, we can eliminate those dependencies by using data with various directions. According to the ray theory (Červený *et al.*, 1977), we can express the path effect in a horizontally layered structure as

$$P_{ij}(f) = R_{ij}^{-1} \exp\left(\frac{-\pi f t_{ij}}{Q_s(f)}\right) \prod_l T_l \left(\frac{\rho_s \beta_s}{\rho_g \beta_g}\right)^{0.5}, \quad (2)$$

where $Q_s(f)$ represents the path-averaged quality factor for S-wave, t_{ij} and R_{ij}^{-1} are the S-wave travel time and the geometrical spreading factor between the i-th event and the j-th station, respectively. T_l is the transmission coefficient at the l-th interface. ρ_s and β_s are the density and the S-wave velocity at the source, and ρ_g and β_g are those at the observation site, respectively. In this study, we calculate R_{ij}^{-1} and T_l by dynamic ray tracing (Červený *et al.*, 1977) assuming the horizontally layered (1-D) velocity structure under the stations (Fig. 2). The 1-D velocity structure is constructed based on the 2-D P-wave velocity (α) structure beneath the southern Kurile trench deduced from ocean bottom seismographic refraction studies (Iwasaki *et al.*, 1989). ρ and β are estimated from the empirical relations; $\rho = 1.7 + 0.2\alpha$ (Červený *et al.*, 1977; Nafe and Drake, 1957) and $\beta = \alpha/\sqrt{3}$.

Since $S_i(f)$ and $G_j(f)$ as well as $Q_s(f)$ affect the characteristics of the observed spectra as shown in Eq. (1), it is impossible to directly evaluate $Q_s(f)$ from the S-wave spectra. Two techniques have been proposed for the Q_s estimation; the spectral inversion method (Iwata and Irikura, 1988) and the coda normalization method (Aki, 1980). Hereafter we abbreviate the spectral inversion method and the coda normalization method as the SI method and the CN method. The SI method can estimate not only $Q_s(f)$ but

$S_i(f)$ and $G_j(f)$ from multi-event and multi-station spectra. On the other hand, the CN method needs single-station spectra from multi-events for the Q_s estimation. A good agreement of the results from the two techniques adds significant confidence in the Q_s estimate. This is a reason why we apply the two techniques for the Q_s estimation.

2.1.1 Spectral inversion method By taking logarithm of Eqs. (1) and (2) we obtain the following equation.

$$\log(O'_{ij}(f)) = \log(S'_i(f)) + \log(G_j(f)) - \log(e)\frac{\pi f t_{ij}}{Q_s(f)} \quad (3)$$

where $O'_{ij} = (R'_{ij}/R_{\text{ref}})O_{ij}$, $S'_i = S_i/R_{\text{ref}}$, $R'_{ij} = R_{ij}(\rho_g \beta_g/\rho_s \beta_s)^{0.5}/(\prod_l T_l)$. R_{ref} is the arbitrary normalizing distance and e is the Napier's number. The unknown parameters, $S_i(f)$, $G_j(f)$ and $Q_s(f)$, are determined by minimizing the residual of Eq. (3) and observed spectra in the least-squares sense. We solve this least-squares problem with two linear inequality constraints ($G_j(f) \geq 2$ and $Q_s^{-1}(f) \geq 1000^{-1}f^{-1}$) using the singular value decomposition method (Lawson and Hanson, 1974). The constraint condition ($G_j(f) \geq 2$) represents the free surface amplification effect.

2.1.2 Coda normalization method Coda waves consist of mainly scattered S-waves. The spectral amplitude of coda waves ($O_{ij}(f, t_c)$) can be expressed from the single-scattering model of Aki and Chouet (1975) as

$$O_{ij}(f, t_c) = S_i(f)G_j(f)P(f, t_c) \quad (4)$$

where $P(f, t_c)$ is the coda excitation factor that is independent of a location relation of hypocenter and station for a lapse time (t_c) greater than about twice the direct S-wave travel time (Aki and Chouet, 1975). By dividing Eqs. (1)
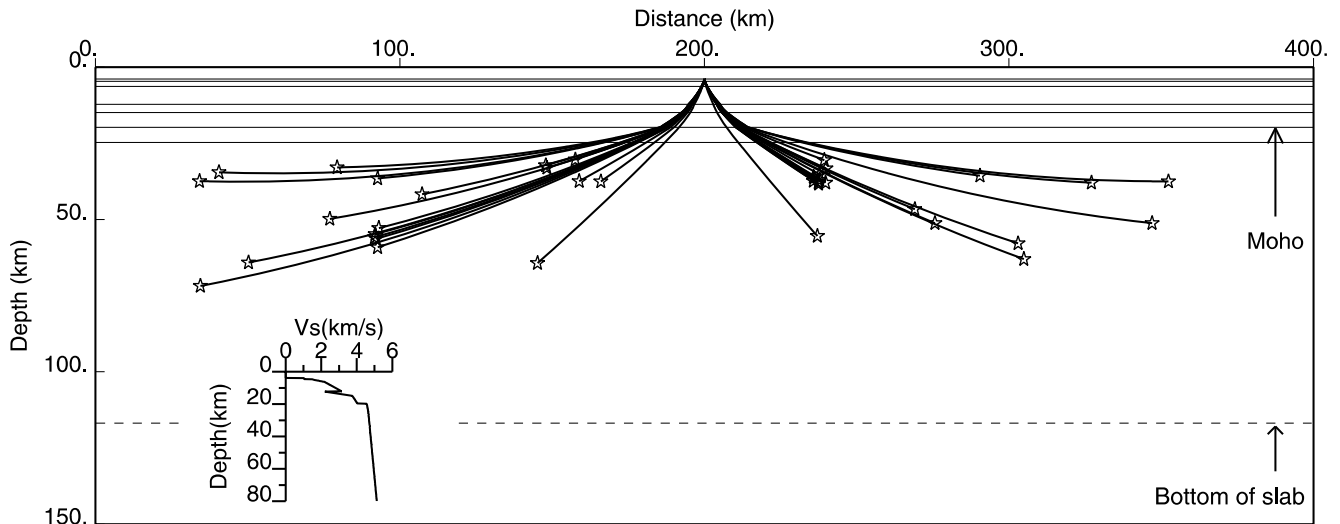
Fig. 2. Diagram of seismic rays from the events (open stars) to OBS2 station. This section runs parallel to the trench. OBS2 is located at the center (200 km point). The S-wave velocity profile assumed is shown in the lower left of the figure. A dashed line roughly indicates the bottom of the slab.
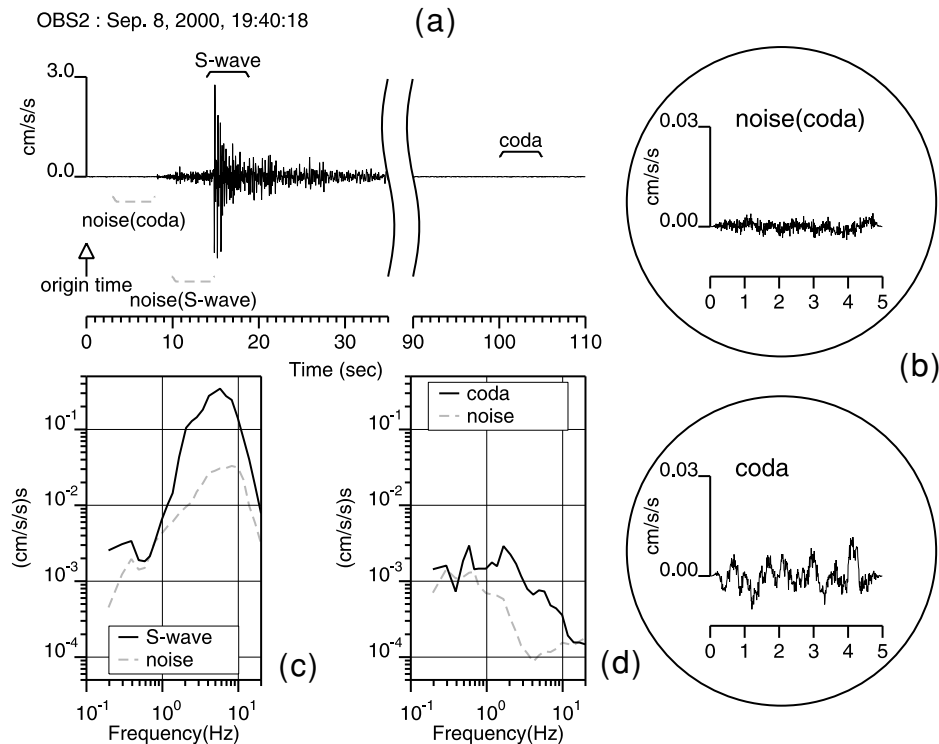

Fig. 3. (a) An example of the observed horizontal-component accelerogram. Time windows for the spectral analysis are also shown; S-wave, coda, noise (S-wave) and noise (coda). Note the discontinuous time axis. (b) Enlarged accelerograms for the windowed coda and noise (coda). Acceleration Fourier amplitude spectra of S-wave and its noise (c) and those of coda and its noise (d) are also shown.

and (2) by Eq. (4) and taking into consideration the hypothesis that $S_i(f)$ and $G_j(f)$ are common to S- and coda wave, we obtain the following equation:

$$\ln\left(\frac{R'_{ij}O_s(f)}{O_c(f,t_c)}\right) = -\pi f t_{ij}/Q_s(f) + \text{const}(f) \quad (5)$$

where $O_s(f)$ and $O_c(f,t_c)$ are the amplitude spectra of the observed S- and coda wave, respectively. Applying the least-squares method to plots of logarithm of coda normalized amplitude (left-hand side of Eq. (5)) against the S-wave

travel time (t_{ij}) for many earthquakes, we can estimate the Q_s value from a slope of the linear regression line.

2.2 Data

In this study, we use the data obtained at two stations (OBS1 and OBS2), which are arranged approximately parallel to the Kurile trench axis (Fig. 1). Since gimbals units are not used in the OBS, the directions of the three axes of each OBS are slightly rotated (Hirata et al., 2002). We use one of two horizontal-component accelerometers; it has a small dip angle ($< 2.3°$).

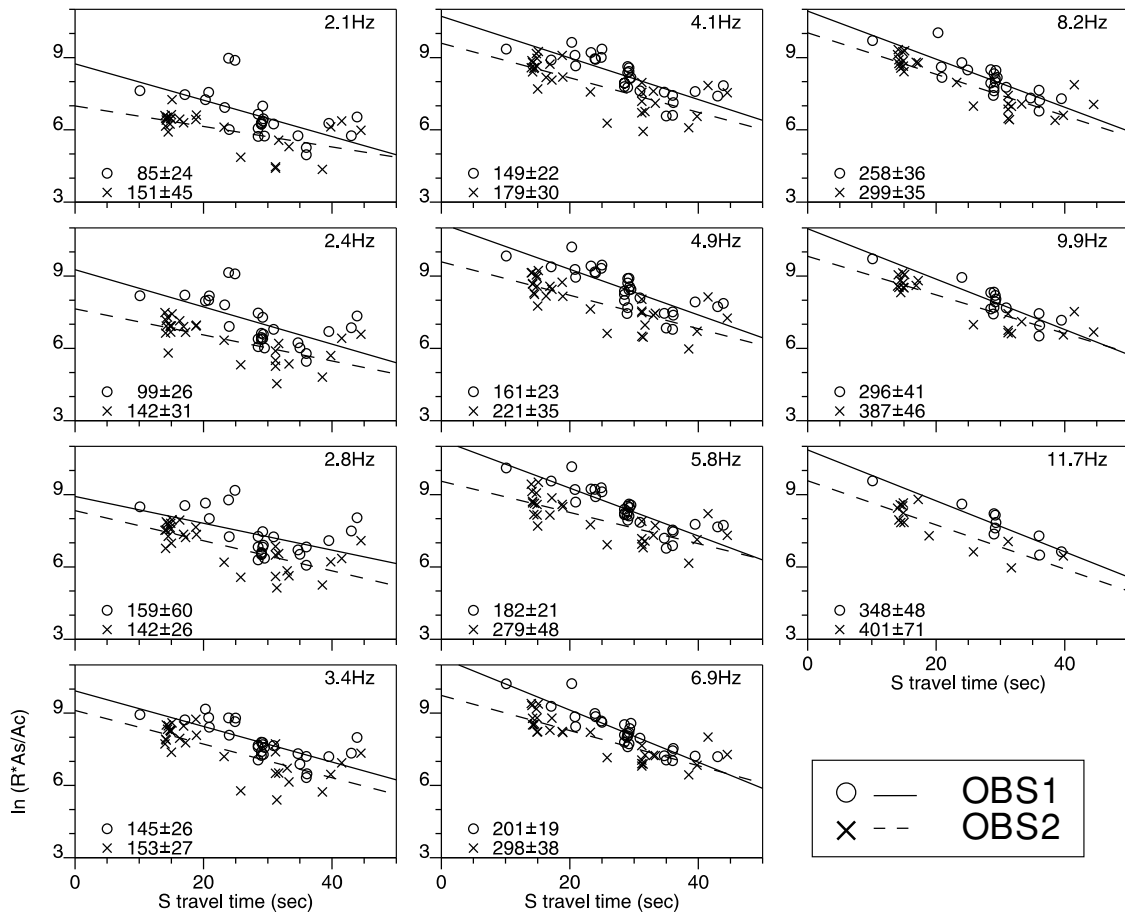We select local earthquakes occurring in a narrow belt,

Fig. 4. Plots of logarithm of coda normalized amplitude against S-wave travel times for selected frequencies. Estimated Q_s values are also shown in each panel.

that is roughly parallel to the trench axis (Fig. 1), during the period of August, 2000 to June, 2002. This belt is set to satisfy two conditions. The first condition is to approximately justify the assumed 1-D velocity structure beneath the belt. The second is applicability of the CN method; we should use data with hypocentral distances less than 200 km (Tsumura, 1967). Figure 1 shows epicenters of the events as well as the stations used. The hypocenter location, origin time and magnitude of these events are taken from the Japan Meteorological Agency (JMA) unified catalogue. For the SI method, 83 records from 50 earthquakes, having magnitudes from 3.0 to 4.8 and focal depths between 30 and 70 km, are analyzed. Five of those events occurred at a depth deeper than 60 km. On the other hand, for the CN method, we analyze 60 records (OBS1: 30, OBS2: 30) from 37 earthquakes having magnitudes from 3.0 to 4.5 and focal depths from 30 to 65 km; these data have S-wave travel times less than 45 sec. Figure 2 shows a diagram of seismic rays from analyzed events to OBS2. It can be seen that the majority of the ray passes through the upper mantle in the slab and that the ray length passing through the crust is nearly the same for all events analyzed. These are the advantage of our dataset.

Figure 3 shows an example of observed acceleration time histories and Fourier amplitude spectra. The time window of about 5-sec with a cosine-shaped taper at 10% each end of the window is used in the spectral analysis. Fourier am-
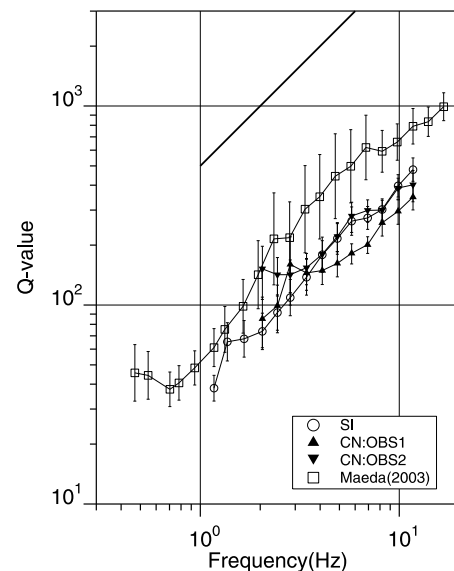

Fig. 5. Summary of Q_s values in the southern Kurile subduction zone. Open circles are Q_s values for the upper layer of the slab estimated by the spectral inversion method, and triangles and invert-triangles are those estimated by the coda normalization method for stations OBS1 and OBS2, respectively. Vertical bars indicate the standard deviation. Open squares are Q_s values for the fore-arc side mantle wedge beneath the eastern Hokkaido (Maeda, 2003). A bold line represents Q_s values for the lower layer of the slab; $Q_s = 500 f^{1.0}$.
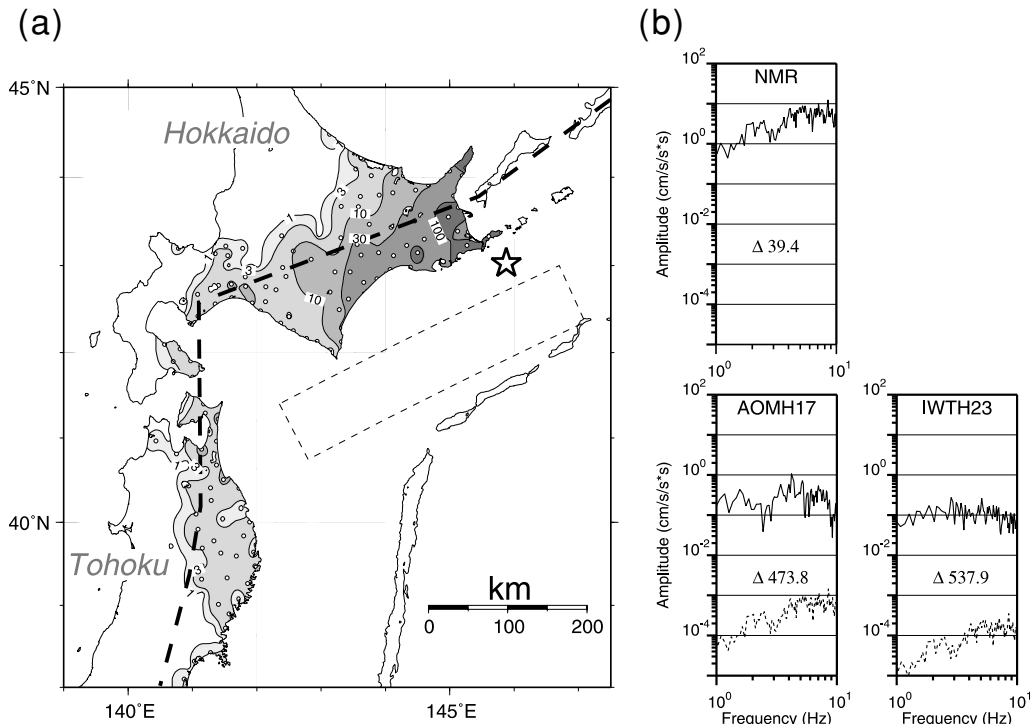
Fig. 6. (a) Distribution of peak ground accelerations (PGAs in cm/sec^2) at K-NET stations (open circles) from the eastern Hokkaido event (April 27, 2001 event; star). The dashed-line rectangle indicates the study zone used in estimation of slab Q_s values. The bold dashed line indicates the volcanic front. (b) Observed S-wave Fourier spectra (bold line) at three stations from the eastern Hokkaido event. The station locations are shown in Fig. 7. The synthetic spectra (dotted line) are also shown at the Tohoku stations (AOMH17 and IWTH23).

plitude spectra of the S-wave and coda wave are calculated by Fast Fourier Transform (FFT). The coda window is set at 100 sec after the event origin time for all events. The logarithms of the amplitude spectra are then smoothed by averaging the amplitudes within the range of $\pm 1/5 f_0$ (f_0, center frequency). The 25 center frequencies are chosen as they are distributed at a common interval from 0.1 to 20 Hz logarithmically. We use only data with a signal-to-noise ratio greater than 2 at each frequency. Two portions of the seismogram, just before the S-wave arrival and the P-wave arrival, are used in calculation of the noise spectra for S-wave and coda wave, respectively (see Fig. 3). The frequency range of the spectrum analysis is limited (about 1 to 12 Hz) due to the low signal-to-noise ratio of the data at the lower- and higher-frequencies (see Figs. 3(c) and (d)). Moreover, for the CN method, data should satisfy a condition that the coda decay curve is independent of a location relation of hypocenter and station at each frequency. This condition limits the analyzing frequency range (2–12 Hz) for the CN method.

3. Results

In the SI method, we constrains the site amplification factor being greater than 2 ($G_j(f) \geq 2$). This constraint is generally needed to remove the trade-off problem between the source and site amplification factors (see Eq. (3)). The inversion result shows the site amplification factors of nearly 2 in the frequency range from 1 to 12 Hz at OBS2. These site amplification factors are not adequate for ocean bottom seismic stations because sedimentary layers exist beneath the stations; the sedimentary layers cause strong

site amplification (Huerta-Lopez *et al.*, 2003). In this case, the inverted source factors are not correct. In spite of these conditions, Q_s values are stably obtained.

In Fig. 4, we show plots of logarithm of coda normalized amplitude against the S-wave travel times at each selected frequency for stations OBS1 and OBS2. We estimate the Q_s value from the slope of the linear regression line (see Eq. (5)) which is evaluated using Deming's method.

Figure 5 is a summary of the results. The open circles show the Q_s values estimated by the SI method, and the triangles and the inverted triangles show those by the CN method for stations OBS1 and OBS2, respectively. The results by two methods show a satisfactory agreement. This adds significant confidence in the estimated Q_s values. At the lower bands (2–3 Hz), the results for station OBS2 by the CN method show a somewhat different feature from the other results. This may be due to the incomplete satisfaction of the condition for coda wave.

The Q_s values increase with frequencies and then we fit a power law to the frequency dependence for the frequency range 1–10 Hz. We obtain $Q_s = 38.6 f^{1.03}$ for the SI method results, and $Q_s = 58.6 f^{0.68}$ and $Q_s = 77.4 f^{0.67}$ for OBS1 and OBS2 results by the CN method. We also obtain $Q_s = 65.6 f^{0.69}$ by averaging the Q_s values for OBS1 and OBS2 results. If we limit the frequency range from 3 to 10 Hz, we get more consistent Q power law results: $Q_s = 55.9 f^{0.70}, 57.8 f^{0.83}$ and $48.8 f^{0.91}$ for OBS1, OBS2 by the CN method, and the SI method, respectively. In the above least-squares estimate, the reciprocal of the standard deviation is used as the weight.

In Fig. 5, the Q_s values of the fore-arc side mantle
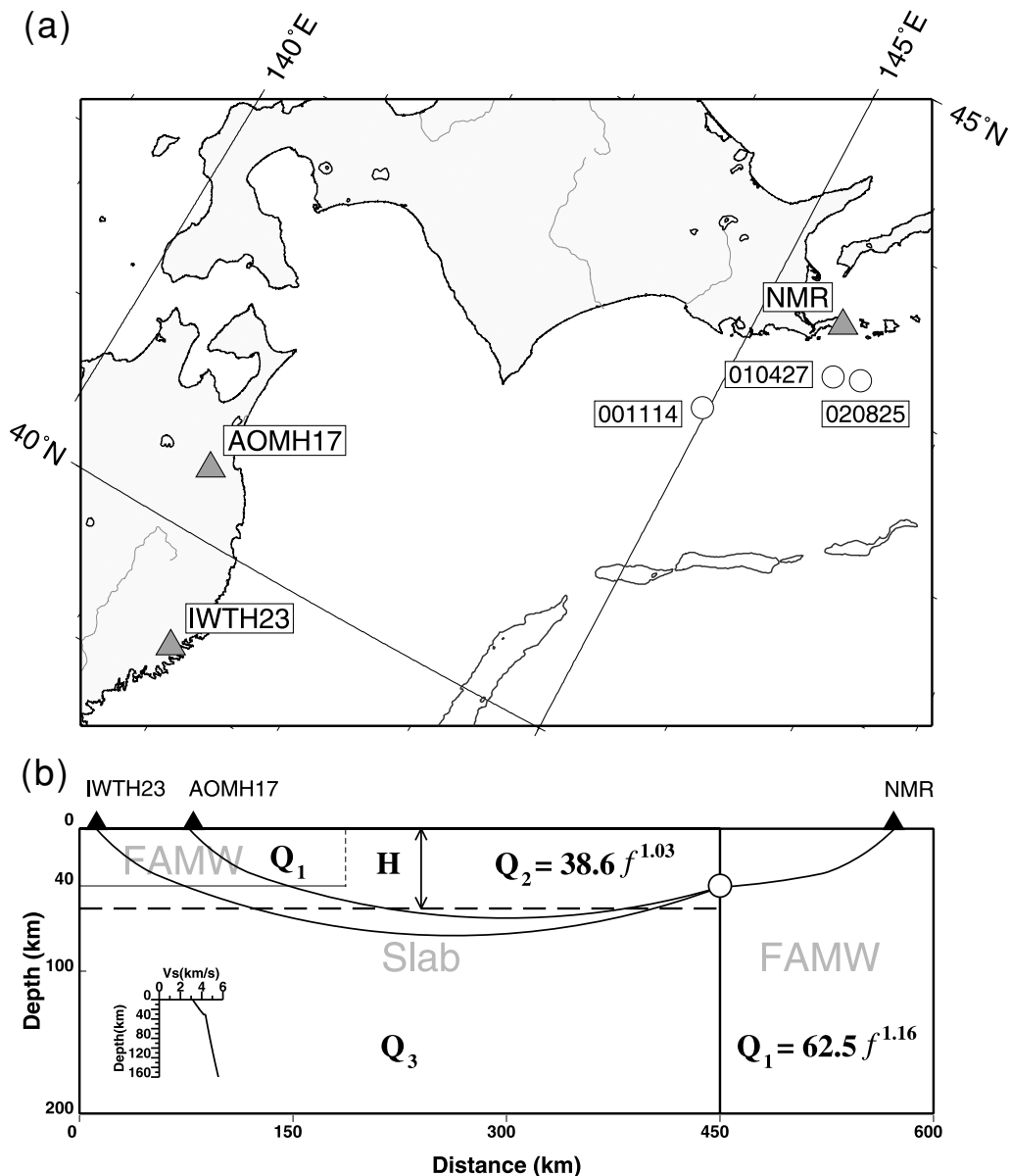
(a)

(b)

Fig. 7. (a) Location map showing stations (triangles) and earthquakes (circles) used in estimation of Q_s values for the lower layer of the slab. (b) Schematic diagram of the two-layer Q_s structure. An open circle and solid triangles are the hypocenter and stations, respectively. Solid curves represent seismic rays calculated by ray tracing for the assumed 1-D velocity structure shown in the inset.

wedge (abbreviation; FAMW, Fig. 1) beneath the eastern Hokkaido, Japan (Maeda, 2003) are also shown by open squares, together with those of the slab. The Q_s values of the FAMW have been estimated by the SI method using strong ground-motion records from earthquakes having focal depths of 100 to 150 km. Strictly speaking, these Q_s values are the path-averaged ones including the mantle wedge and the slab; however the seismic rays pass mainly through the mantle wedge. Figure 5 shows that the slab Q_s values are slightly smaller than those of the FAMW. This seems to contradict the previous studies that showed the high Q_s values of the slab. We discuss this issue in the next section.

4. Two-layer Q_S Structure of the Slab

At island-arc regions, an abnormal distribution of seismic intensities is observed during interplate and intraslab earthquakes (e.g., Utsu, 1967). Figure 6(a) shows a typical ex-

ample of the abnormal distribution of ground motion from an intraslab event (April 27, 2001; depth 80 km, M_W 6.0) beneath the eastern Hokkaido. Here the distribution of peak ground accelerations (PGAs) instead of seismic intensities is depicted using the dense K-NET strong-motion network (Kinoshita, 1998) of National Research Institute for Earth Science and Disaster Prevention (NIED). We can point out two abnormal phenomena of the PGA distribution. One is strong attenuation of PGAs at the back-arc side of the volcanic front in Hokkaido; this is explained by low Q_s values in the back-arc side mantle wedge (Utsu, 1967; Maeda, 2003). The other is large PGAs at the fore-arc side of the volcanic front in Tohoku in spite of a large epicentral distance ($\sim$500 km). This abnormal distribution of ground motion shown in Fig. 6(a) is observed during any earthquakes occurring beneath the eastern Hokkaido and the reciprocal relation is also observed for earthquakes occurring beneath
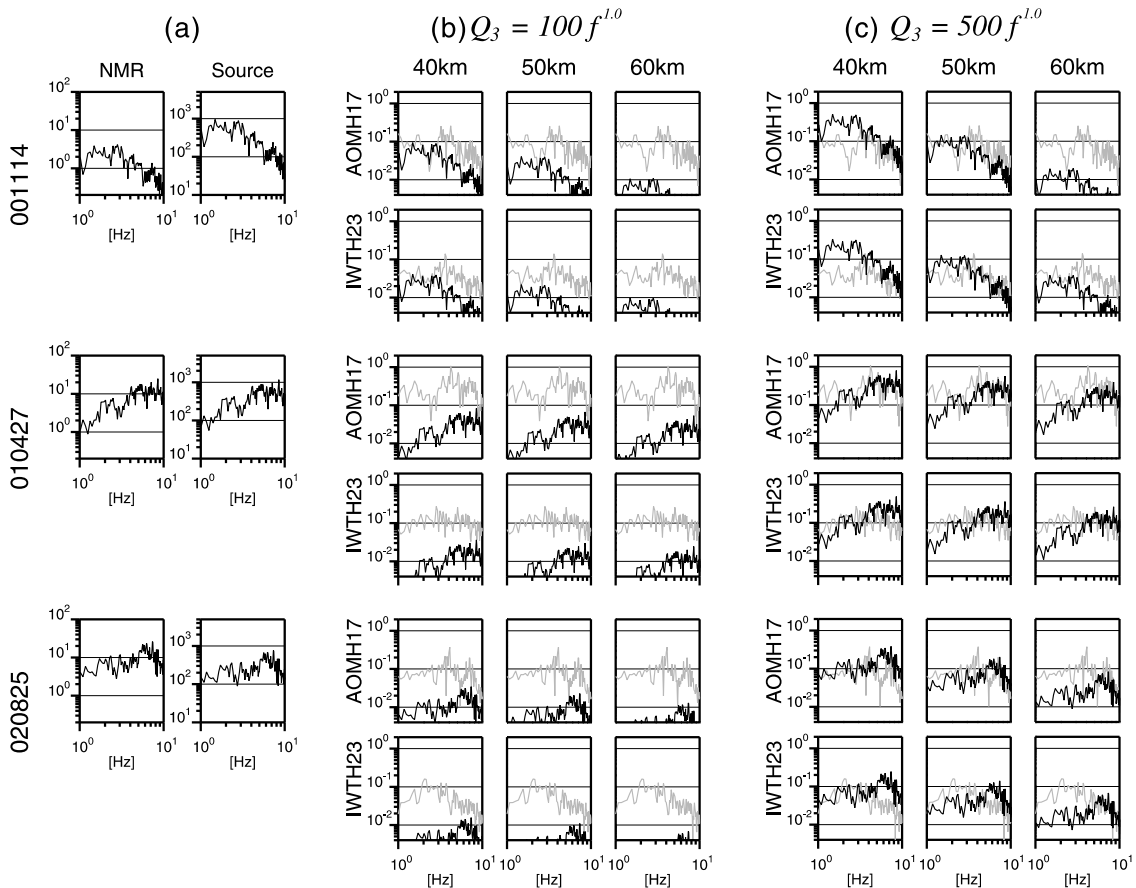
Fig. 8. (a) Left: observed S-wave spectra for three events at NMR. Right: S-wave source spectra for the three events estimated from the NMR spectra. (b) Comparison between the observed (gray line) and synthetic (solid line) spectra at AOMH17 and IWTH23. The synthetic spectra are calculated for $Q_3 = 100 f^{1.0}$ and $H = 40$, 50 and 60 km where Q_3 and H are Q_s values for the lower layer of the slab and the boundary depth between the upper and lower layer (see Fig. 7). (c) Same as (b), but for $Q_3 = 500 f^{1.0}$.

the eastern Tohoku. Although these abnormally large PGAs have been explained by the high Q slab in the previous studies, our slab Q_s values are not high enough to explain this phenomenon. Actually, as shown in Fig. 6(b), the synthetic S-wave spectra at the Tohoku stations by using our slab Q_s values ($38.6 f^{1.03}$) are smaller by about three-order than the observed ones; the synthetic method is mentioned later in this section.

Here we propose a two-layer Q_s structure of the slab to explain the both facts, our slab Q_s values and the abnormally large PGAs in Tohoku for the eastern Hokkaido events. The seismic rays for most of earthquakes used in our analysis pass through the upper part of the slab as shown in Fig. 2. On the other hand, the seismic rays from the eastern Hokkaido event to Tohoku shown in Fig. 6(a) pass through the deeper part of the slab and the large PGAs in Tohoku result from these rays. Thus it is natural that the two-layer Q_s structure consists of the upper layer with not so high Q_s values and the lower layer with very high Q_s values. In the following, we roughly estimate the slab Q_s structure based on strong motion data at the eastern Hokkaido and Tohoku stations from the eastern Hokkaido events.

Figure 7(a) shows locations of the earthquakes and stations used in the analysis. NMR is an F-net station (Fukuyama *et al.*, 1996) of NIED. The strong motion velocity seismometer is installed in the observational vault exca-

vated in the Cretaceous hard mud or sandstone. We assume a surface S-wave velocity at NMR to be 1.7 km/sec based on the nearby borehole PS-logging data. This station is used to estimate the source spectra of the events. AOMH17 and IWTH23 are KiK-net stations (Aoi *et al.*, 2000) of NIED, where the strong motion accelerometers are equipped at the ground surface and borehole bottom (about 100 m depth); that is, a vertical array. Since the PS-logging data are available at the KiK-net stations, we can estimate an incident wave at the borehole bottom by removing the effects of surface layers overlaying the borehole accelerometer. S-wave velocities at the borehole-bottom are 1.45 km/sec and 2.20 km/sec at AOMH17 and IWTH23, respectively. We can assume that the estimated incident waves at these stations are records on the rock site as NMR. We use these records (estimated incident waves) in the following analysis.

Figure 7(b) shows a schematic diagram to model the two-layer Q_s structure. This diagram is made based on the slab configuration beneath the study area. An open circle and solid triangles indicate the hypocenter and stations, respectively. The right-hand side region of the hypocenter corresponds to the FAMW of the eastern Hokkaido and $Q_1 = 62.5 f^{1.16}$ is assumed for this region (Maeda, 2003; Fig. 5); the seismic rays from the events to NMR mainly pass through the FAMW. On the other hand, the left-hand side region of the hypocenter corresponds to the slab and

$Q_2 = 38.6 f^{1.03}$ is assumed for the upper layer. We simply model the FAMW of the Tohoku region as shown in Fig. 7(b); the Tohoku FAMW has the same Q_s values as the eastern Hokkaido. The geometrical spreading factor as well as the ray path is calculated by the dynamic ray tracing for the 1-D velocity structure (an inset in Fig. 7(b)) that roughly explains observed S-wave travel times for events occurring in the study region. The boundary depth (H) between the upper and lower layer and the Q_s values (Q_3) of the lower layer are unknowns to be solved. The H and Q_3 are estimated by comparing the synthetic and observed S-wave spectra at the Tohoku stations for the eastern Hokkaido events.

The synthetic S-wave spectra at the Tohoku stations are calculated by the following procedure (Fig. 8). First we estimate the source spectrum for each event from the observed S-wave spectrum at NMR. The S-wave spectrum is calculated by FFT using the time window of 10.24 sec with a cosine-shaped taper at 10% each end of the window. The source spectrum is obtained by de-convolving the observed spectrum for the site and path effects (geometrical spreading and inelastic-attenuation effects) (see Eq. (1)). The site amplification at NMR is assumed to be 2 for all frequencies. Next, we calculate the synthetic S-wave spectra at the borehole bottom of stations AOMH17 and IWTH23 by convolving the above source spectrum with the path effect of the two-layer slab. The trials of the two-layer Q_s structure are made for the various combinations of H and Q_3. The range for H is 30 km to 80 km at intervals of 10 km, and assumed values for Q_3 are $100f$, $200f$, $500f$ and $1000f$; here we simply assume the power law frequency dependence of Q_3 values, $Q_3 = Q_0 f^{1.0}$. The total attenuation effect due to the upper and lower layer is evaluated based on the ray path passing through each layer. This procedure is also used to estimate the synthetic spectra shown in Fig. 6(b); in this case, we assume a single layer slab.

The incident S-wave spectra at the borehole bottom of stations AOMH17 and IWTH23 are estimated from the observed ground-surface spectra by correcting the site amplification effects. The site amplification effects are evaluated by using the Propagator Matrix method (e.g., Aki and Richards, 1980) and the S-wave velocity structure assuming the vertical incident SH wave.

Finally, we compare the synthetic spectra for various combinations of H and Q_3 with estimated incident spectra at stations AOMH17 and IWTH23, and then select H and Q_3 that give a good agreement between them for three events. In Fig. 8, an example of the comparison is shown for $H = 40, 50, 60$ km and $Q_3 = 100f, 500f$. This figure shows that $H = 50$ km and $Q_3 = 500f$ give the reasonably good agreement for three events. The Q_s values of the lower layer are also depicted in Fig. 5. The lower layer has quite high Q_s values compared with the other regions. Our Q_s values of the lower layer consist with those by Nakamura and Uetake (2000); their Q_s values at 7 Hz are 2000–3000 for the depth range from 60 to 90 km beneath our study area.

5. Discussions

In this paper, we proposed the two-layer Q_s structure of the slab near the southern Kurile trench. The upper layer has not so high Q_s values; this was first discovered here by using the OBS data. The lower layer has very high Q_s values as previously estimated by using land-station data. The boundary between the upper and lower layer in our two-layer Q_s structure is sharp; however, we don't assert it because the estimation method is rough one. An important point is that the Q_s values of the lower layer are higher by one-order than those of the upper layer (Fig. 5). Around the study zone, the thickness of the Pacific slab is about 100 km and earthquakes occur within the top 50 km of the slab as shown in Fig. 9. It is interesting to point out that earthquakes occur only in the upper layer of the two-layer Q_s structure of the slab near the southern Kurile trench. This may mean that the two-layer Q_s structure reflects the different material property between the upper and lower layer of the slab.

It is well known that oceanic S wave is high-frequency seismic phase which propagates over distances greater than $30°$ in the oceanic lithosphere. Butler *et al.* (1987) obtained frequency dependent Q_s values of oceanic S ($Q_s \approx 180 f^{1.1}$) in the western Pacific. Kubo *et al.* (1995) also obtained Q_s values of oceanic S ($Q_s \approx 500f$) in the north-
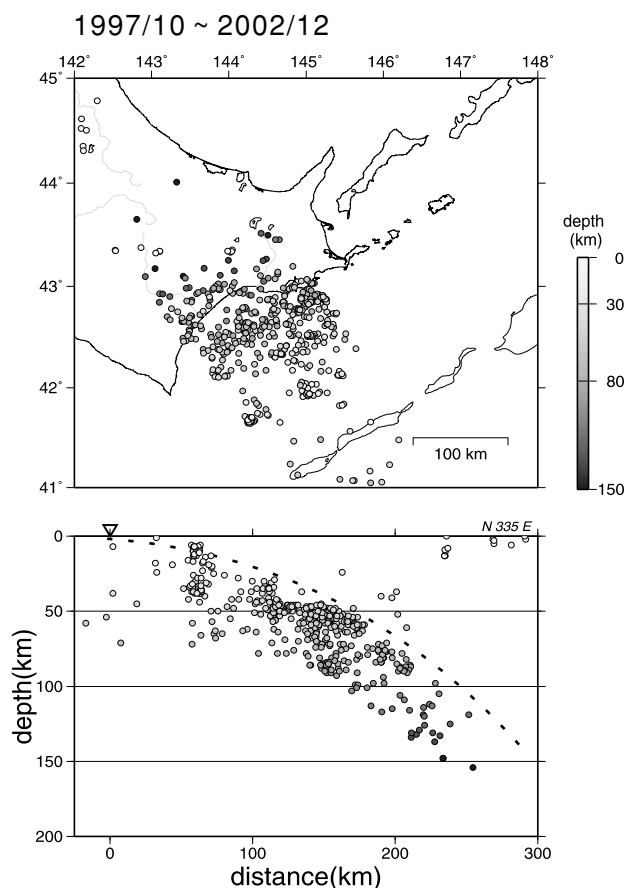

Fig. 9. Hypocenter distribution around the study area in the southern Kurile subduction zone. Upper: epicenter distribution. Lower: vertical section perpendicular to the trench axis (inverted triangle). A dashed curve shows the rough upper boundary of the Pacific slab. The hypocenter data are taken from JMA unified catalogue.
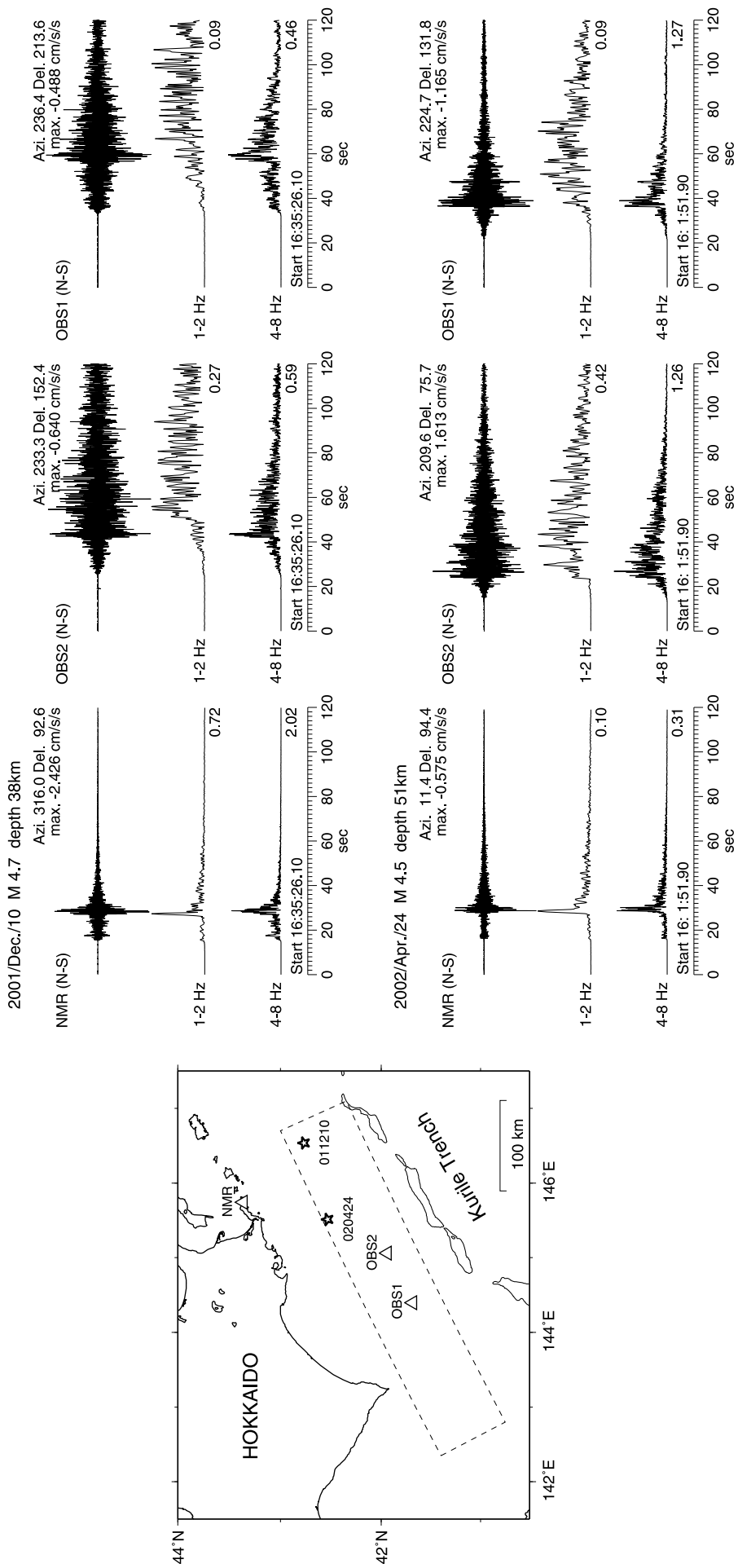
Fig. 10. Comparison between acceleration waveforms (upper traces) and band-pass filtered envelopes (middle and lower traces) at NMR and ocean bottom stations (OBS1 and OBS2) from two events. The map inset shows the stations and epicenters used. Note different coda wave decay between the NMR and ocean bottom stations.

western Pacific. These Q_s values are obviously higher than those of the upper layer and nearly the same as those of the lower layer of the slab near the southern Kurile trench. Talandier and Bouchon (1979) discussed a mechanism of oceanic S propagation and proposed guided waves within the lower lithosphere as its mechanism. If this is true, it is a natural consequence that the Q_s values of oceanic S wave are similar to the lower layer Q_s values of the slab.

Seismic attenuation is considered to be caused by two mechanisms, intrinsic and scattering mechanisms (Sato and Fehler, 1998); intrinsic attenuation converts wave energy into heat, while scattering attenuation just redistributes wave energy within the medium. From the characteristics of coda wave as well as direct waves, we can speculate the dominant attenuation mechanism of the medium (Fehler *et al.*, 1992; Hoshiba, 1993). Figure 10 shows acceleration waveforms and band-pass filtered envelopes of two events at three stations (NMR, OBS1 and OBS2). The seismic ray from the event to NMR mainly passes through the FAMW, but that from the event to OBS passes through the slab. The envelopes at NMR show large amplitudes at direct S-wave arrival and rapidly decaying coda wave for every frequency, while those at the OBS stations show more slowly decaying coda wave than NMR. These evidences suggest that the scattering attenuation is more effective within the slab in comparison with the FAMW. The slower rate of coda decay is also caused by the structurally trapped waves or excited modes (Phillips and Aki, 1986). At the OBS stations, such near site resonance effect is possible since sedimentary layers exist beneath the stations. The coda envelope shapes at the OBS stations vary with the frequency range. In the 1–2 Hz range, the coda envelopes have larger amplitude than the direct wave, and show very long duration. These low-frequency coda shapes may reflect the near site resonance effects. Next issue is to construct the heterogeneous slab structure that induces seismic wave attenuation due to the scattering mechanism. Recently Furumura and Kennett (2005) have addressed this issue.

6. Conclusion

We estimated Q_s values of the subducting Pacific slab near the southern Kurile trench. We used especially the seismic data from OBS stations because the seismic rays pass mainly through the slab. Two techniques of Q_s estimation were applied to these data. The estimated Q_s values from the two methods are nearly the same and increase with frequencies: for the frequency rage from 1 to 10 Hz, $Q_s = 38.6 f^{1.03}$ by the spectral inversion method and $Q_s = 65.6 f^{0.69}$ by the coda normalization method. However, these Q_s values are not high enough to explain the abnormal distribution of ground motion (abnormal distribution of seismic intensities). Thus we proposed the two-layer Q_s structure of the slab to explain the both facts, our slab Q_s values and the abnormal distribution of ground motion. The two-layer Q_s structure consists of the upper layer with not so high Q_s values and lower layer with very high Q_s values (about $500 f^{1.0}$); the upper layer has a thickness of about 50 km. We pointed out that the two-layer Q_s structure reflected the different material property between the upper and lower layer of the slab.

References

Aki, K., Attenuation of shear-waves in the lithosphere for frequencies from 0.05 to 25 Hz, *Phys. Earth Planet. Inter.*, **21**, 50–60, 1980.

Aki, K. and B. Chouet, Origin of coda waves: source, attenuation and scattering effects, *J. Geophys. Res.*, **80**, 3322–3342, 1975.

Aki, K. and P. G. Richards, *Quantitative Seismology. vol. 1*, 557 pp., W. H. Freeman and Company, 1980.

Aoi, S., K. Obara, S. Hori, K. Kasahara, and Y. Okada, New strong-motion observation network: KiK-net, *EOS Trans. AGU*, 329, 2000.

Butler, R., C. S. McCreery, L. N. Frazer, and D. A. Walker, High-frequency seismic attenuation of oceanic P and S waves in the Western Pacific, *J. Geophys. Res.*, **92**, 1383–1396, 1987.

Červený, V., I. A. Molotkov, and I. Pšenčík, *Ray Method in Seismology*, 214 pp., Univerzita Karlova, Praha, 1977.

Fehler, M., M. Hoshiba, H. Sato, and K. Obara, Separation of scattering and intrinsic attenuation for the Kanto-Tokai region, Japan, using measurements of S-wave energy versus hypocentral distance, *Geophys. J. Int.*, **108**, 787–800, 1992.

Fukuyama, E., M. Ishida, S. Hori, S. Sekiguchi, and S. Watada, Broadband seismic observation conducted under the FREESIA Project, *Rep. Natl. Res. Inst. Earth Sci. Disaster Prev.*, **57**, 23–31, 1996.

Furumura, T. and B. L. N. Kennett, Subduction zone guided waves and the heterogeneity structure of the subducted plate: intensity anomalies in northern Japan, *J. Geophys. Res.*, **110**, B10302, doi:10.1029/2004JB003486, 2005.

Hirata, K., M. Aoyagi, H. Mikada, K. Kawaguchi, Member, IEEE, Y. Kaiho, R. Iwase, S. Morita, I. Fujisawa, H. Sugioka, K. Mitsuzawa, K. Suyehiro, H. Kinoshita, and N. Fujiwara, Real-time geophysical measurements on the deep seafloor using submarine cable in the southern Kurile subduction zone, *IEEE J. Ocean. Eng.*, **27**(2), 170–181, 2002.

Hoshiba, M., Separation of scattering attenuation and intrinsic absorption in Japan using the multiple lapse time window analysis of full seismogram envelope, *J. Geophys. Res.*, **98**, 15809–15824, 1993.

Huerta-Lopez, C., J. Pulliam, and Y. Nakamura, In situ evaluation of shear-wave velocities in seafloor sediments with a broadband ocean-bottom seismograph, *Bull. Seism. Soc. Am.*, **93**, 139–151, 2003.

Iwasaki, T., H. Shiobara, A. Nishizawa, T. Kanazawa, K. Suyehiro, N. Hirata, T. Urabe, and H. Shimamura, A detailed subduction structure in the Kuril trench deduced from ocean bottom seismographic refraction studies, *Tectonophysics*, **165**, 315–336, 1989.

Iwata, T. and K. Irikura, Source parameters of the 1983 Japan Sea earthquake sequence, *J. Phys. Earth*, **36**, 155–184, 1988.

Kinoshita, S., Kyoshin Net (K-NET), *Seism. Res. Lett.*, **69**, 309–332, 1998.

Kubo, A., T. Ouchi, and H. Shimamura, Envelope broadening and spatial attenuation of S-waves in the oceanic lithosphere, *Mem. Grad. School Sci. and Technol., Kobe Univ.*, **13-A**, 101–116, 1995.

Lawson, C. L. and R. J. Hanson, *Solving Least Squares Problems*, 340 pp., Prentice-Hall, Inc., Englewood Cliffs, New Jersey, 1974.

Maeda, T., A study on characteristics of seismic wave attenuation and seismic source in the subduction zone, Doctoral dissertation, Hokkaido University, Sapporo, Japan, 134 pp., 2003 (in Japanese).

Nafe, J. E. and C. L. Drake, Physical properties of crustal materials as related to compressional wave velocities, paper presented at Annual Meeting of Soc. Expl. Geophys., Dallas, Texas, 1957.

Nakamura, R. and T. Uetake, Three dimensional attenuation structure and

site amplification inversion by using a large quantity of seismic strong motion records in Japan, paper presented at 12th World Conference on Earthquake Engineering, Auckland, New Zealand, Jan. 30 to Feb. 4, 2000, ID 0724.

Phillips, W. and K. Aki, Site amplification of coda waves from local earthquakes in central California, *Bull. Seism. Soc. Am.*, **76**, 627–648, 1986.

Sato, H. and M. C. Fehler, *Seismic Wave Propagation and Scattering in the Heterogeneous Earth*, 308 pp., AIP Press/Springer Verlag, New York, 1998.

Talandier, J. and M. Bouchon, Propagation of high frequency Pn wave at great distances in the central and south Pacific and its implications for the structure of the lower lithosphere, *J. Geophys. Res.*, **84**, 5613–5619, 1979.

Tsumura, K., Determination of earthquake magnitude from total duration of oscillation, *Bull. Earthq. Res. Inst. Univ. Tokyo*, **45**, 7–18, 1967.

Tsumura, N., S. Matsumoto, S. Horiuchi, and A. Hasegawa, Three-dimensional attenuation structure beneath the northeastern Japan arc estimated from spectra of small earthquakes, *Tectonophysics*, **319**, 241–260, 2000.

Umino, N. and A. Hasegawa, Three-dimensional Q_s structure in the northeastern Japan arc, *Zisin II*, **37**, 217–228, 1984 (in Japanese with English abstract).

Utsu, T., Anomalies in seismic wave velocity and attenuation associated with a deep earthquake zone, *J. Fac. Sci., Hokkaido Univ., Ser. VII (Geophys.)*, **3**, 1–25, 1967.

Wessel, P. and W. H. Smith, New version of the Generic Mapping Tools released, *EOS Trans. AGU*, **329**, 1995.

T. Maeda (e-mail: tmaeda@ares.sci.hokudai.ac.jp) and T. Sasatani